This is the accepted manuscript made available via CHORUS. The article has been published as:

Semiempirical *ab initio* modeling of bound states of deep defects in semiconductor quantum technologies

YunHeng Chen, Lachlan Oberg, Johannes Flick, Artur Lozovoi, Carlos A. Meriles, and Marcus W. Doherty

Phys. Rev. B **109**, L201115 — Published 15 May 2024

DOI: 10.1103/PhysRevB.109.L201115

Semi-empirical *ab initio* modeling of bound states of deep defects in semiconductor quantum technologies

YunHeng Chen,[1] Lachlan Oberg,[1] Johannes Flick,[2,3,4] Artur Lozovoi,[3] Carlos A. Meriles,[3,4] and Marcus W. Doherty[1]

[1] *Department of Quantum Science and Technology, Research School of Physics, Australian National University, Canberra, Australian Capital Territory 2601, Australia*
[2] *Center for Computational Quantum Physics, Flatiron Institute, New York, NY 10010, U.S.A*
[3] *Department of Physics, CUNY-City College of New York, New York, NY 10031, U.S.A*
[4] *CUNY-Graduate Center, New York, NY 10016, U.S.A*

(Dated: April 17, 2024)

A significant hurdle in developing high-performance semiconductor quantum technologies utilizing deep defects is related to charge dynamics. Unfortunately, progress in modeling their charge dynamics has been hindered over recent decades due to the absence of appropriate multiscale models capable of accurately representing the atomic properties of these defects and their impact on device performance. Here, we present a semi-*ab initio* method for modeling the bound states of deep defects in semiconductor quantum technologies, applied to the negatively charged nitrogen vacancy (NV^-) center in diamond. We employ density functional theory calculations to construct accurate potentials for an effective mass model, which allow us to unveil the structure of the bound hole states. We develop a model to calculate the non-radiative capture cross-sections, which agrees with experiment within one order of magnitude. Finally, we present the first attempt at constructing the photoionization spectrum of $NV^0 \rightarrow NV^- +$ bound hole, showing that the electronic transitions of the bound holes can be distinguished from phonon sidebands. This work offers a practical and efficient solution to a long-standing challenge in understanding the charge dynamics of deep defects.

I. INTRODUCTION

Deep defects are essential in semiconductor quantum technologies (SQT), finding diverse applications in quantum computing, sensing and communication [1–11]. Deep defects can exist in multiple charge states, posing a significant challenge for developing high-performance SQT due to the complexities of their charge dynamics [1, 2, 12–14]. Unfortunately, progress in modeling the charge dynamics of deep defects has stagnated over the past few decades due to the inherently complex multiscale problem, wherein atomic properties have a profound impact on macroscopic outcomes. Existing methods such as density functional theory (DFT) [15] offer insights at the atomic scale but are limited by computational constraints, making them unsuitable for describing highly excited orbitals in larger volumes. On the other hand, phenomenological models lack the necessary atomic-level understanding to accurately predict properties such as capture cross-sections and the photoionization spectrum. Overcoming these critical obstacles will significantly enhance the performance of SQT using deep defects.

In this work, we overcome these deficiencies by presenting a semi-*ab initio* model of the bound states of deep defects in semiconductor quantum technologies. For demonstration, we apply this model to the NV^- center in diamond [1]. We first simulate the discretized energies of the bound hole states by adopting an effective mass Hamiltonian and use DFT to accurately describe the effective potential of NV^-. We then model the non-radiative capture of charge carriers by applying a deformation potential model of acoustic and optical hole-phonon scattering. Our results show that the simulated capture cross-sections differ from experimental results by only one order of magnitude due to the exclusion of two-phonon Raman processes. Finally, we construct the photoionization spectrum of $NV^0 \rightarrow NV^- +$ bound hole by evaluating the transition dipole moments using a combination of effective mass theory and DFT and by estimating the phonon sidebands (PSB). We show that the electronic transitions of the bound hole states are indeed distinguishable from the PSBs.

II. EFFECTIVE MASS HAMILTONIAN

In diamond, the valence band maximum (VBM) is triply degenerate [16], where we approximate that the VBM consists of two degenerate heavy hole (HH) bands and a single light hole (LH) band. We simulate the energy levels of the bound hole states by adopting an effective mass Hamiltonian. This method assumes the solutions can be well approximated by an envelope wavefunction multiplied by a Bloch function [17]. The coupling between each band is ignored for simplicity and to avoid ambiguities in the definition of the Bloch function basis when constructing the effective potential. The wavefunction solutions are given by

$$\psi_{b,i}\left(\vec{r}\right) = F_{b,i}\left(\vec{r}\right) u_b\left(\vec{r}\right) \tag{1}$$

where $u_b\left(\vec{r}\right)$ is the periodic Bloch function of the b^{th} band at the valence band maximum (VBM) at the Γ point of the unperturbed diamond structure, and $F_{b,i}\left(\vec{r}\right)$ is the slowly-varying envelope wavefunction of the b^{th} band of the i^{th} level. This approximation is valid if the envelope

wavefunction varies slowly within the primitive unit cell [17].

Using the assumptions outlined above, we construct a Schrödinger equation for the envelope wavefunction by taking the expectation value of the physical Hamiltonian with respect to the Bloch functions over the volume of a primitive unit cell and assigning an isotropic effective mass (m_b) to each of the bands. Accordingly, the Schrödinger equation is given by [18]

$$\left(\frac{\vec{p}^2}{2m_b} + \Delta V_b\left(\vec{r}\right)\right) F_{b,i}\left(\vec{r}\right) = \Delta E_{b,i} F_{b,i}\left(\vec{r}\right) \tag{2}$$

where

$$\Delta V_b\left(\vec{r}\right) = \frac{1}{V_c}\int_{-\infty}^{\infty} \left|f_b\left(\vec{r'}\right)\right|^2 \Delta V\left(\vec{r'}+\vec{r}\right) d^3r' \tag{3}$$

The first and second term in Eq. 2 are the kinetic energy operator with an effective hole mass tensor and the effective potential of the b^{th} band, respectively. In Eq. 3, $f_b\left(\vec{r'}\right)$ is the Bloch function $u_b\left(\vec{r'}\right)$ within the central unit cell and is enforced to be zero outside of that volume of the unit cell, thereby allowing the integral limits to be expanded to all space. $\Delta V\left(\vec{r}\right) = V_{\mathrm{NV}^-}\left(\vec{r}\right) - V_{\mathrm{diamond}}\left(\vec{r}\right)$ is the effective potential defined by the difference between the potential generated by a NV^- center ground state and a defect-free diamond. Note that $u_b\left(\vec{r}\right)$ are the solutions to a perfect diamond. $\Delta E_{b,i} = E_{b,i} - E_{\mathrm{VBM}}$ is the difference in energy between the solution of the effective mass equation ($E_{b,i}$) and the recombination energy of NV^0 ($E_{\mathrm{VBM}} = 2.94$ eV) [19].

III. CONSTRUCTING EFFECTIVE POTENTIAL

We adopt the frozen core approximation to define the effective potential. This assumes that the state of the electron at the NV center is not affected by the state of the hole, so the potential experienced by the hole is described by the electrostatic potential generated by the nuclei and electrons. However, this approximation explicitly ignores exchange-correlation interactions between the bound hole and the electrons in the NV center.

We construct the effective potential by employing DFT to obtain the electron charge densities and nuclear geometries of these two systems. The primitive unit cell of diamond consists of two atoms, and they contribute to the charge densities at the VBM. For demonstration purposes, we evaluate $\Delta V_b\left(\vec{r}\right)$ by approximating the probability density of VBM $\left|f_b\left(\vec{r'}\right)\right|^2$ as a single Gaussian function (see Supplemental Material Sec. IB [18]).

After creating the near-field effective potential using DFT, the next step is to extrapolate it to larger volumes. While we anticipate the far-field potential to resemble that of a point charge due to the NV^- center's effective single electron charge, there is also an intermediate-field potential that deviates from this behavior. To capture this potential, we solve the Poisson's equation in COMSOL Multiphysics® to obtain the intermediate-field potential.

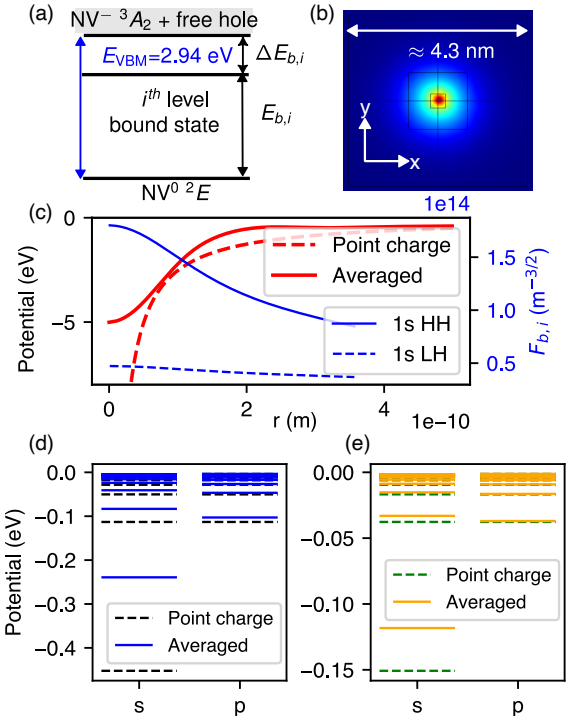


FIG. 1: Simulation of bound hole states. (a) Schematic description of the bound hole states. The shaded region denotes the continuum levels of valence band states. (b) Wavefunction of the ground bound hole state simulated using COMSOL. (c) Comparison of a spherically averaged potential and a point charge potential in diamond and the $l = 0$ radial envelope wavefunctions for HH and LH. The radial wavefunctions are plotted over the dimension of a primitive unit cell with a radius of 3.567Å. (d) Comparison of the $l = 0$ and 1 bound HH and (e) LH states (solid lines) with a hydrogenic model (dashed lines) using the stated effective masses.

IV. SIMULATION OF BOUND HOLE STATES

We solve Eq. 2 using 3 different methods. Firstly, we use COMSOL simulations with a Dirichlet boundary condition and an isotropic effective mass to obtain the low lying excited states (ES). However, directly obtaining the higher excited bound hole states via COMSOL simulations is computationally inefficient due to the large spatial extent of their wavefunctions. Thus, we use a spherically averaged effective potential to solve for the radial Schrödinger equation to obtain the higher ES. Lastly, we benchmark the solutions of the first two methods using

a simple hydrogenic model.

Fig. 1b shows the ground state (GS) energy due to a HH, obtained from COMSOL simulations. The simulation used isotropic effective masses of $1.08m_e$ and $0.36m_e$ for the heavy and light hole mass, respectively (where m_e is the mass of the electrons [18]) over a dimension of $214.5 \times 214.5 \times 214.5$ Å^3. The GS energy is -0.24 eV below E_{VBM}. We achieve mesh convergence with deviations of less than 1% for both HH and LH solutions and cell convergence with errors of less than 7%(3%) up to 30(5) levels for HH(LH) solutions. Using $E_{\mathrm{VBM}} = 2.94$ eV [19], we find the GS simulated using our methods (-0.24 eV) to be in good agreement with the energy obtained via *ab initio* calculations (-0.27 eV) [20]. As the exchange-correlation potential is not captured in our EMA model, this result sets an upper limit of 0.03 eV on the effects of exchange-correlation which decrease as the hole orbit gets larger.

Comparing the spherically averaged solutions to COMSOL, COMSOL observes additional splittings due to the true C_{3v} symmetry of the defect, unlike the former. However, HH and LH solutions between these methods vary by less than 3% when ignoring these splittings and considering mean values of energy levels [18]. This agreement prompts us to examine the spherically averaged solutions, revealing a hydrogenic-like potential at large distances. This implies that higher ES solutions will be well approximated by a hydrogenic series [Fig. 1c]. Comparing eigenenergies of HH and LH with a hydrogenic model, the higher ES with azimuthal quantum number $l = 0$ and 1 indeed closely follow a hydrogenic series, unlike the lower ES [Fig. 1d, 1e]. Our simulations confirm the validity of using EMA since the radial wavefunctions exhibit minimal changes within the primitive unit cell, except for the GS where solution accuracy may diminish. [Fig. 1c]. Moreover, this method is efficient and enables us to access higher excited bound hole states that are otherwise unattainable in three-dimensional simulations.

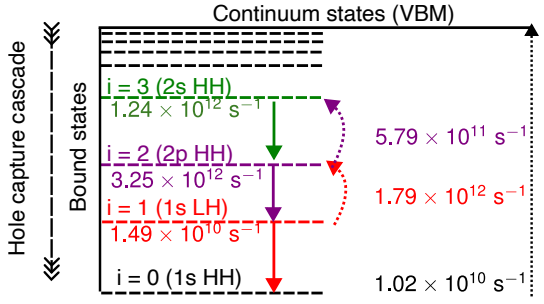


FIG. 2: Schematics for hole cascade capture process via emission of phonons. Solid and dotted lines, along with their respective values denote the emission rates and absorption rates, respectively.

V. CAPTURE CROSS-SECTION

We now model the non-radiative capture of the holes by applying the deformation potential model of hole-acoustic/optical phonon scattering (see Supplemental Material Sec. V [18].) The hole capture cross-section can be determined rigorously using the cascade trapping framework, mediated by the emission of phonons [17, 21, 22]. The capture process occurs when phonon emission is much faster than absorption, such that the bound hole has a negligible chance of excitation. The critical transition occurs from the first ES to the GS. As we will be showing later, we consider this transition to be the capture event as the absorption of phonons out from the GS is slower than the emission of phonons to the GS from the first ES. Our previous work which utilized a brute-force Monte Carlo simulations [12] demonstrated that multiple inelastic scattering events helped the system to reach the critical transition at room temperature. Consequently, the justification for this hole capture model, contingent upon the ability of a hole to cascade down to this critical transition, is firmly established.

We calculate the scattering rates for all possible direct transitions from and to the GS, first ES and the ns HH states ($n = 2 - 5$) [18]. We find that the scattering rates are decreasing with increasing n. However, the asymptotic limit of the rates is unclear due to limited datasets [18]. We observe that the direct emission rate from the first ES to the GS is faster compared to the total absorption rate out from the GS [Fig. 2]. Hence, the emission rate of this critical transition is effectively the hole capture rate. As the emission rate of the first ES is slower than the absorption rate to the second ES, we can then assume that thermal equilibrium (TE) has been established within the ES before it makes the critical transition down to the GS. Subsequently, the capture rate is approximated as the sum of the total emission rate from all the ES to the GS, multiplied by the partition function.

The capture cross-section σ_{cap} can be defined as [23]

$$\sigma_{\mathrm{cap}} = \frac{V\Gamma_{\mathrm{cap}}}{\nu} \tag{4}$$

where ν is the hole thermal velocity in diamond, V is the volume of the system and Γ_{cap} is the hole capture rate. Assuming the TE approximation, both bound and free hole states are considered in the entire diamond, with the latter being dominant. Hence, the total partition function Z_{tot} is the sum of the partition functions due to the bound states Z_{B} and the free hole states Z_{F}.

By converting the discrete sum of wavevectors into a continuous variable, Z_{F} is proportional to V. We adopt the partition function of a hydrogen atom for the bound state [24] and we terminate the sum over the bound states by the maximum principal quantum number that corresponds to the wavefunctions which fits within V, determined by the Bohr's radius of the wavefunction. Subsequently, Z_{B} is proportional to $V^{1/3}$. In the limit of

large V, the contribution of Z_{B} is negligible compared to Z_{F} and thus the capture cross-section, valid at room temperature is approximately [18]

$$\sigma_{\mathrm{cap}} \approx \frac{8}{\nu} e^{-\beta E_1} \left(\pi\kappa\beta\right)^{3/2} \sum_{b,i_{\mathrm{B}}} e^{-\beta \Delta E_{b,i_{\mathrm{B}}}} \Gamma_0^{b,i_{\mathrm{B}}} \qquad (5)$$

where E_1 is the energy of the first ES, $\beta = 1/k_B T$ in which k_B is the Boltzmann constant and T is the temperature. κ is the curvature averaged over the HH and LH bands at the VBM. $\Delta E_{b,i_{\mathrm{B}}}$ is the energy difference between the i^{th} bound state and E_1 and $\Gamma_0^{b,i_{\mathrm{B}}}$ denotes all possible direct emission rates from the higher bound states to the GS permitted by the phonon energies. Eq. 5 is a physically valid expression that doesn't depend on the volume of the system.

The capture cross-section at $T = 300$ K is $1.65 \times 10^{-4} \mu\mathrm{m}^2$, approximately one order of magnitude smaller than the experimental value [20]. One-phonon process dominates at low temperatures [25] whereas two-phonon processes dominate at room temperature [1]. The discrepancy in our calculations is attributed to the exclusion of two-phonon processes in the scattering rate calculations. Two-phonon emission rates will be larger due to the additional decay pathways accessible through the combination of a thermally driven and a spontaneous transition. However, this is not the case for absorption processes which necessitate two thermally driven transitions. At room temperature, such thermal processes are significantly slower than the dominant spontaneous emission transitions, as the relevant phonon energy is much larger than the thermal energy. Thus, the capture rate is expected to increase due to higher overall emission rate. Consequently, we underestimated the calculated capture cross-sections. To prevent divergence at the low-temperature limit, we will need to include the contributions from the bound states to Eq. 5 which is now volume-dependent.

VI. PHOTOIONIZATION SPECTRUM OF $NV^0 \rightarrow NV^- +$ BOUND HOLES

We now turn to modeling the photoionization spectrum of $NV^0 \rightarrow NV^- +$ bound holes. It is impossible to directly model this using *ab initio* techniques due to computational constraints. Instead, we make an approximation by adopting the Huang-Rhys model to describe the zero-phonon lines (ZPL) and the PSBs [17]. The spectrum can be obtained by evaluating the transition dipole moment, constructing the vibrational overlap functions and subsequently evaluating the absorption cross-section [18]. The bound state solutions are represented by Eq.1. The observed transition is the transition of a hole from the e orbital of NV^0 to the bound state. Here, we assume that the e orbital of NV^0 is sufficiently localized that it is only non-zero over the dimension of the NV^- center. In this region, it is suitable to perform Taylor series expansion on the dipole moment transition matrix elements $\left(\vec{D}_{b,i}\right)$ in terms of the envelope wavefunctions obtained from the bound state simulations and the integrals over e orbital and $u_b(\vec{r})$, which are evaluated using DFT. In this work, we only deal with the zero-order term and thus limit ourselves to transitions involving s-like orbitals.

The presence of an NV center reduces the cubic symmetry of diamond to C_{3v} symmetry and splits the triply degenerate states at Γ point of the VBM to a pair of doubly degenerate states and one single degenerate state. Using DFT, we identified two degenerate transitions originating from the valence band states to the e_y orbital of NV^0, which corresponds to HH. However, LH transition could not be identified. We then averaged the absolute square of the transition dipole moments from the doubly degenerate valence band states, yielding a parallel-to-transverse component ratio of 0.32. Consequently, the absorption cross-section is polarization-independent [18].

Taking into account the Stokes shift (ΔE_S), the absorption cross-section consisting of ZPL and PSBs, summed over all possible transitions at energy $E_{b,i}$ is given by

$$\sigma(E) = 4\pi^2 \chi \sum_{b,i} E \overline{\left|\vec{D}_{b,i}\right|^2} \Bigg(L\left(E - E_{b,i} + \Delta E_S, \Gamma_{b,i}\right) + P\left(E - E_{b,i} + \Delta E_S, T\right) \Bigg) \qquad (6)$$

where $\chi = e^2/4\pi\epsilon\hbar c$ is the fine structure constant of diamond, L is ZPL of each transition, P is the vibrational overlap functions and $\overline{\left|\vec{D}_{b,i}\right|^2}$ is the averaged transition dipole matrix elements. Both features are explicitly weighted by the exponent of the temperature-dependent Huang-Rhys factor (S).

We make the following assumptions to obtain the absorption cross-sections. First, we validated the similarities of the phonon modes of the internal transitions of NV^- and $NV^0 \rightarrow NV^- + h^+$ using DFT, which agree to 71%. Consequently, we can construct the PSBs of the $NV^0 \rightarrow NV^- +$ bound holes by using the known generating function of the NV^- PSBs [26], combined with an estimate of the Huang-Rhys factor and the evaluated energies of those transitions. Second, using DFT and conventional methods, we obtained the low-temperature Huang-Rhys factor of $S_0 = 0.942$ for the $NV^0 \rightarrow NV^- + h^+$ (free hole) transition with the assumption of C_{3v} symmetry and have explicitly neglected the Jahn-Teller effect. We adopted the Huang-Rhys factor for the transitions involving the bound states. Finally, we modified S [27] and constructed the PSBs accordingly at $T = 5$ K and $T = 300$ K, as depicted in Fig. 3.

We model the ZPL of each transition with a Lorentzian function. The Lorentzian function has a linewidth defined by the total scattering rate ($\Gamma_{b,i}$) from each transition due to the absorption and emission rate as obtained from the hole-acoustic/optical phonon scattering model [18]. We have explicitly neglected the recombi-

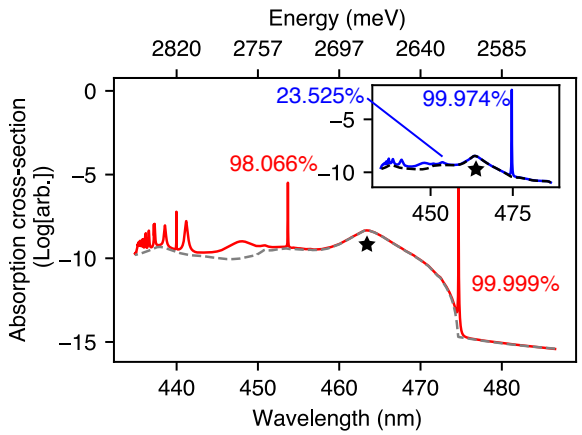


FIG. 3: Absorption cross-section at $T = 5$ K plotted on a logarithmic scale and renormalized relative to the highest peak of the spectrum. The solid lines represent the full photoionization spectrum whereas the dotted lines are the PSBs. The PSBs for wavelength greater than 475 nm at $T = 5$ K have been reconstructed to prevent divergence on the logarithmic scale. The star signs denote the phonon sideband peak at 463 nm. The percentages indicate the fidelities of exciting a ZPL peak, labelled for the first and second bound hole transitions. Inset: absorption cross-section at $T = 300$ K.

nation rate as we expect the recombination to be much slower than other broadening processes. For energy levels that have not been explicitly calculated, we assume that their linewidths exhibit a scattering rate that is similar to that of the preceding energy level. Additionally, we approximate the GS scattering rate at low temperature to be limited by the lifetime of the ES which is typically on the order of 10 ns [1].

The electronic transitions of the bound states can be distinguished from the PSBs as seen in Fig. 3. However, it's crucial to note that there is a PSB peak at 463 nm, which may be misidentified as a ZPL. For Rydberg-like schemes, the ability to selectively excite a specific electronic transition is crucial. The key measure is the fidelity of exciting a ZPL peak compared to the phonon sideband beneath it. The calculated high selectivity at low temperatures is promising for the potential application of Rydberg-like schemes.

VII. CONCLUSION

In summary, we presented a semi-*ab initio* model for simulating the bound states of deep defects in semiconductor quantum technologies, which we applied to the NV^- center in diamond. We quantitatively showed the model's prediction of the lowest bound state energy to be in good agreement with direct *ab initio* simulations. We used the solutions of the bound states to model hole capture cross-section which agrees with experimens within one order of magnitude and to construct the first prediction of photoionization spectrum of $NV^0 \rightarrow NV^- +$ bound hole. These models represent a critical advancement to a long-standing challenge in understanding deep defects' charge dynamics. However, additional work is admittedly in order. This includes a better description of the probability density of VBM charge densities, incorporating two-phonon Raman processes in the scattering rate calculations, and accurate modeling of NV^0 PSBs.

ACKNOWLEDGMENTS

A.L. and C.A.M acknowledge support from the National Science Foundation through grants NSF-2216838 and NSF-1914945; they also acknowledge access to the facilities and research infrastructure of the NSF CRE,ST IDEALS, grant number NSF-2112550. M.W.D. acknowledges support from the Australian Research Council DE170100169. The Flatiron Institute is a division of the Simons Foundation.

[1] M. W. Doherty, N. B. Manson, P. Delaney, F. Jelezko, J. Wrachtrup, and L. C. L. Hollenberg, The nitrogen-vacancy colour centre in diamond, Phys. Rep. **528**, 1 (2013).
[2] D. D. Awschalom, R. Hanson, J. Wrachtrup, and B. B. Zhou, Quantum technologies with optically interfaced solid-state spins, Nat. Photonics **12**, 516 (2018).
[3] S. Wehner, D. Elkouss, and R. Hanson, Quantum internet: A vision for the road ahead, Science **362**, eaam9288 (2018).
[4] Y. Chen, S. Stearn, S. Vella, A. Horsley, and M. W. Doherty, Optimisation of diamond quantum processors, New J. Phys. **22**, 093068 (2020).
[5] S. Pezzagna and J. Meijer, Quantum computer based on color centers in diamond, Appl. Phys. Rev. **8**, 011308 (2021).
[6] C. T. Nguyen, D. D. Sukachev, M. K. Bhaskar, B. Machielse, D. S. Levonian, E. N. Knall, P. Stroganov, R. Riedinger, H. Park, M. Lončar, and M. D. Lukin, Quantum network nodes based on diamond qubits with an efficient nanophotonic interface, Phys. Rev. Lett. **123**, 183602 (2019).
[7] M. K. Bhaskar, R. Riedinger, B. Machielse, D. S. Levonian, C. T. Nguyen, E. N. Knall, H. Park, D. Englund, M. Lončar, D. D. Sukachev, and M. D. Lukin, Experimental demonstration of memory-enhanced quantum communication, Nature **580**, 60 (2020).
[8] A. Lohrmann, B. C. Johnson, J. C. McCallum, and S. Castelletto, A review on single photon sources in silicon carbide, Rep. Prog. Phys. **80**, 034502 (2017).

[9] N. T. Son, C. P. Anderson, A. Bourassa, K. C. Miao, C. Babin, M. Widmann, M. Niethammer, J. Ul Hassan, N. Morioka, I. G. Ivanov, F. Kaiser, J. Wrachtrup, and D. D. Awschalom, Developing silicon carbide for quantum spintronics, Appl. Phys. Lett. **116**, 190501 (2020).

[10] A. B. D. Shaik and P. Palla, Optical quantum technologies with hexagonal boron nitride single photon sources, Sci. Rep. **11**, 12285 (2021).

[11] A. E. Naclerio and P. R. Kidambi, A review of scalable hexagonal boron nitride (h-bn) synthesis for present and future applications, Adv. Mater. **35**, 2207374 (2023).

[12] A. Lozovoi, Y. Chen, G. Vizkelethy, E. Bielejec, J. Flick, M. W. Doherty, and C. A. Meriles, Detection and modeling of hole capture by single point defects under variable electric fields, Nano Lett. **23**, 4495 (2023).

[13] N. T. Son and I. G. Ivanov, Charge state control of the silicon vacancy and divacancy in silicon carbide, J. Appl. Phys. **129**, 215702 (2021).

[14] A. Gale, D. Scognamiglio, I. Zhigulin, B. Whitefield, M. Kianinia, I. Aharonovich, and M. Toth, Manipulating the charge state of spin defects in hexagonal boron nitride, Nano Lett. **23**, 6141 (2023).

[15] R. O. Jones, Density functional theory: Its origins, rise to prominence, and future, Rev. Mod. Phys. **87**, 897 (2015).

[16] O. Madelung, *Semiconductors: Data Handbook* (Springer, 2004) p. 691.

[17] A. M. Stoneham, *Theory of defects in solids* (Clarendon Press, 2001) p. 955.

[18] See Supplemental Material for *ab initio* calculations, additional simulations of the potentials, bound hole states and scattering rates, as well as the theoretical descriptions of an effective mass model, deformation potential model of hole-phonon scattering, capture cross-sections and the photoionization spectrum of $NV^0 \rightarrow NV^- +$ bound hole state. The Supplemental Material also contains Refs. [1,16,17,23,24,26,28-50]

[19] N. Aslam, G. Waldherr, P. Neumann, F. Jelezko, and J. Wrachtrup, Photo-induced ionization dynamics of the nitrogen vacancy defect in diamond investigated by single-shot charge state detection, New J. Phys. **15**, 013064 (2013).

[20] A. Lozovoi, H. Jayakumar, D. Daw, G. Vizkelethy, E. Bielejec, M. W. Doherty, J. Flick, and C. A. Meriles, Optical activation and detection of charge transport between individual colour centres in diamond, Nature Electronics **4**, 717 (2021).

[21] M. Lax, Cascade capture of electrons in solids, Phys. Rev. **119**, 1502 (1960).

[22] D. R. Hamann and A. L. McWhorter, Cascade capture of electrons by ionized impurities, Phys. Rev. **134**, A250 (1964).

[23] A. Alkauskas, Q. Yan, and C. G. Van de Walle, First-principles theory of nonradiative carrier capture via multiphonon emission, Phys. Rev. B **90**, 075202 (2014).

[24] W. Ebeling, W.-D. Kraeft, and G. Röpke, On the quantum statistics of bound states within the rutherford model of matter, Ann. Phys. **524**, 311 (2012).

[25] T. Astner, J. Gugler, A. Angerer, S. Wald, S. Putz, N. J. Mauser, M. Trupke, H. Sumiya, S. Onoda, J. Isoya, J. Schmiedmayer, P. Mohn, and J. Majer, Solid-state electron spin lifetime limited by phononic vacuum modes, Nat. Mater. **17**, 313 (2018).

[26] P. Kehayias, M. W. Doherty, D. English, R. Fischer, A. Jarmola, K. Jensen, N. Leefer, P. Hemmer, N. B. Manson, and D. Budker, Infrared absorption band and vibronic structure of the nitrogen-vacancy center in diamond, Phys. Rev. B **88**, 165202 (2013).

[27] M. L. Goldman, M. W. Doherty, A. Sipahigil, N. Y. Yao, S. D. Bennett, N. B. Manson, A. Kubanek, and M. D. Lukin, State-selective intersystem crossing in nitrogen-vacancy centers, Phys. Rev. B **91**, 165201 (2015).

[28] G. Kresse and J. Furthmüller, Efficient iterative schemes for ab initio total-energy calculations using a plane-wave basis set, Phys. Rev. B **54**, 11169 (1996).

[29] G. Kresse and J. Hafner, Ab initio molecular-dynamics simulation of the liquid-metal–amorphous-semiconductor transition in germanium, Phys. Rev. B **49**, 14251 (1994).

[30] G. Kresse and J. Furthmüller, Efficiency of ab-initio total energy calculations for metals and semiconductors using a plane-wave basis set, Comput. Mater. Sci. **6**, 15 (1996).

[31] G. Kresse and D. Joubert, From ultrasoft pseudopotentials to the projector augmented-wave method, Phys. Rev. B **59**, 1758 (1999).

[32] J. P. Perdew, K. Burke, and M. Ernzerhof, Generalized gradient approximation made simple, Phys. Rev. Lett. **77**, 3865 (1996).

[33] A. Szabo and N. S. Ostlund, *Modern quantum chemistry : introduction to advanced electronic structure theory* (Dover Publications, 1996) p. 466.

[34] P. Atkins and R. Friedman, *Molecular quantum mechanics* (Oxford ; New York : Oxford University Press, 2011).

[35] B. K. Ridley, *Quantum Processes in Semiconductors* (Oxford University Press, 2013) p. 488.

[36] C. Jacoboni and L. Reggiani, The monte carlo method for the solution of charge transport in semiconductors with applications to covalent materials, Rev. Mod. Phys. **55**, 645 (1983).

[37] H. J. McSkimin and P. Andreatch, Elastic moduli of diamond as a function of pressure and temperature, J. Appl. Phys. **43**, 2944 (1972).

[38] J. L. Warren, J. L. Yarnell, G. Dolling, and R. A. Cowley, Lattice dynamics of diamond, Phys. Rev. **158**, 805 (1967).

[39] W. Weber, Adiabatic bond charge model for the phonons in diamond, si, ge, and $\alpha - Sn$, Phys. Rev. B **15**, 4789 (1977).

[40] M. Schwoerer-Böhning, A. T. Macrander, and D. A. Arms, Phonon dispersion of diamond measured by inelastic x-ray scattering, Phys. Rev. Lett. **80**, 5572 (1998).

[41] T. Kazimierczuk, D. Fröhlich, S. Scheel, H. Stolz, and M. Bayer, Giant rydberg excitons in the copper oxide cu2o, Nat **514**, 343 (2014).

[42] J. Heckötter, M. Freitag, D. Fröhlich, M. Aßmann, M. Bayer, M. A. Semina, and M. M. Glazov, Scaling laws of rydberg excitons, Phys. Rev. B **96**, 125142 (2017).

[43] M. Aßmann and M. Bayer, Semiconductor rydberg physics, Adv. Quantum Technol. **3**, 1900134 (2020).

[44] F. Schweiner, J. Main, and G. Wunner, Linewidths in excitonic absorption spectra of cuprous oxide, Phys. Rev. B **93**, 085203 (2016).

[45] H. Stolz, F. Schöne, and D. Semkat, Interaction of rydberg excitons in cuprous oxide with phonons and photons: optical linewidth and polariton effect, New J. Phys. **20**, 023019 (2018).

[46] T. Kitamura, M. Takahata, and N. Naka, Quantum number dependence of the photoluminescence broadening of excitonic rydberg states in cuprous oxide, J. Lumin. **192**, 808 (2017).

[47] M. A. M. Versteegh, S. Steinhauer, J. Bajo, T. Lettner, A. Soro, A. Romanova, S. Gyger, L. Schweickert, A. Mysyrowicz, and V. Zwiller, Giant rydberg excitons in cu_2O probed by photoluminescence excitation spectroscopy, Phys. Rev. B **104**, 245206 (2021).

[48] A. V. Krukau, O. A. Vydrov, A. F. Izmaylov, and G. E. Scuseria, Influence of the exchange screening parameter on the performance of screened hybrid functionals, J. Chem. Phys. **125**, 224106 (2006).

[49] J. Zhang, C.-Z. Wang, Z. Zhu, Q. H. Liu, and K.-M. Ho, Multimode jahn-teller effect in bulk systems: A case of the Nv^0 center in diamond, Phys. Rev. B **97**, 165204 (2018).

[50] G. Davies, Vibronic spectra in diamond, J. Phys. C: Solid State Phys. **7**, 3797 (1974).